Published in final edited form as:
J Orthop Res. 2012 February ; 30(2): 280–287. doi:10.1002/jor.21513.

Morphology of the human vertebral endplate

Azucena G. Rodriguez[1], **Ana E. Rodriguez-Soto**[2], **Andrew J. Burghardt**[2], **Sigurd Berven**[1], **Sharmila Majumdar**[2], and **Jeffrey C. Lotz**[1]

[1]Department of Orthopaedic Surgery, University of California, San Francisco CA 94143, USA

[2]Department of Radiology, University of California, San Francisco, CA 94143 USA

Abstract

It is presumed that poor intervertebral disc cell nutrition is a contributing factor in degeneration, and is exacerbated by vertebral endplate sclerosis. Yet, quantitative relationships between endplate morphology and degeneration are unavailable. We investigated how endplate bone microstructure relates to indices of disc degeneration, such as morphologic grade, proteoglycan content, and cell density.

Intervertebral core samples [n=96, 14 subjects, L1–L5 level, ages 35–85 (64±16 yrs.), degeneration grade 1(n=4), grade 2(n=32), grade 3(n=44), grade 4(n=10), grade 5(n=6)] that included subchondral bone, cartilage endplate and adjacent nucleus were harvested from human cadaveric lumbar spines. The morphology of the vertebral endplate was analyzed using μCT and the adjacent nucleus tissue was collected for biochemical and cellular analyses. Relationships between vertebral endplate morphology and adjacent disc degeneration were analyzed.

Contrary to the prevailing notion, vertebral endplate porosity increased between 50 and 130% and trabecular thickness decreased by between 20 and 50% with advancing disc degeneration ($p<0.05$). We also observed that nucleus cell density increased ($R^2=0.33$, $p<0.05$) and proteoglycan content decreased ($R^2=0.47$, $p<0.05$) as the endplate became more porous.

Our data suggest that endplate sclerosis is not a fundamental factor contributing to disc degeneration. Rather, the opposite was observed in our samples, as the endplate became progressively more porous with age and degeneration. Since ischemic disc cell behavior is commonly associated with degenerative change, this may be related to other factors such as the quality of vertebral capillaries, as opposed to decreased permeability of intervening tissues.

Keywords

spine; vertebra; bone; vertebral endplate; morphology

Introduction

Low back pain is one of the most prominent diseases in industrialized countries (1). U.S. statistics indicate that 80% of the population experience low back pain in their lives, with 40% of cases attributed to degenerative disc disease (DDD) (2). DDD is a normal phenomenon in humans that is strongly associated with aging (3). Pathologic degeneration is the premature loss of architectural, biological, and biomechanical properties of the intervertebral disc (4) that can lead to chronic low back pain. Risk factors for premature degeneration are not fully understood, but include familial predisposition, extreme

Corresponding Author: Jeffrey C. Lotz, Ph.D., Department of Orthopaedic Surgery, University of California, San Francisco, 533 Parnassus Ave, U-453, Box 0514, San Francisco, CA 94143, fax: 415.476.1128, Ph: 415.476.7881, lotzj@orthosurg.ucsf.edu.

mechanical exposures (i.e. occupational lifting or vibration)(5), and poor disc cell nutrition(6). Since the disc is avascular, its cells rely primarily on diffusion for nutrient and waste transport(6, 7).

Nutrients for nucleus cells originate at vertebral capillaries, pass through endplate bone and cartilage, and then diffuse through nucleus matrix (7, 8). Reduced permeability of these tissues that separate vertebral capillaries and disc cells will, theoretically, diminish nutrient availability and hamper disc cell function (9), potentially accelerating degenerative change. Pathologic features that may hamper transport include cartilage endplate calcification (10) and vertebral bone sclerosis (11–13).

Previous research has demonstrated age-related macrostructural changes of the endplate that are linked to disc degeneration(7, 11) suggesting that it thickens by gradual cartilage calcification(11, 14). By contrast, endplate thickness has been correlated with nuclear proteoglycan content, indicating that stress-induced remodeling leads to endplate thinning with increasing disc degeneration (14). This later observation is supported by mechanical testing, which shows a significant decrease of endplate stiffness and strength in vertebra adjacent to more degenerated discs (15, 16). In addition to potential thickness variations, subtle changes in bone microstructure that include porosity, trabecular thickness, pore thickness, and pore number, may also have profound effects on transport (17, 18). Yet, quantitative analysis of these features has not been reported and may provide new insights into the endplate's role in promoting disc degeneration.

We hypothesized that changes in endplate microstructure alter nutrient diffusion, and thereby contribute to disc degeneration. To test this, we examined the relationship between several measures of bone microstructure (bone porosity, trabecular thickness, pore thickness, and pore number) and three disc degeneration indices: MRI-based degeneration grade(19), cell density and nucleus proteoglycan content. We also studied the relationship between the endplate bony morphology and hydraulic permeability.

Methods

Fourteen cadaveric lumbar spines L1–L4 (4) or L1–L5 (10) were obtained from donor banks (4 female and 10 male donors; mean age 64 ± 16 yrs., age range 35–85). The spines were scanned in a 3T MRI Scanner (GE Healthcare, Milwaukee, WI), and graded (on a five-point scale) by 3 trained radiologists using the MRI-based Pfirrmann degeneration criteria (19). Next, the surrounding soft tissue and posterior elements were removed using a bone saw (Exakt Model, Band Saw, Norderstedt, Germany). Fifty-one motion segments were then cut transversely to obtain specimens consisting of half-vertebra/disc/half-vertebra. While frozen to preserve nuclear tissue integrity, the motion segments were cored at the center of the nucleus pulposus using an 8.25 mm diamond coring tool (#102095, Starlite Industries, Rosemont, PA) oriented perpendicular to the endplate surface (Figure 1A) to obtain 102 cylindrical specimens. Only central endplate cores were evaluated since this region is considered most critical for nucleus cell nutrition (20). This core diameter was chosen since it meets the minimum previously reported value used to successfully measure the bone tissue permeability(21). In the transverse plane, nucleus tissue was separated into three equal regions: the central one-third and two endplate-adjacent portions. Each core was composed of the inferior vertebral endplate cranial to the disc, the intervertebral disc nuclear tissue and the superior vertebral endplate caudal to the disc.

Imaging

The vertebral bone cores were thawed and imaged in a commercial micro-computed tomography system (μCT 40, Scanco Medical, Brüttisellen, Switzerland) with an X-ray tube

voltage of 70 kV and 180° acquisition. Each core was placed in a cylindrical sample holder in a bath of protease inhibitors diluted 1:10 with distilled water (P2714 Protease inhibitor cocktail, Sigma-Aldrich, St Louis MO) to keep the cartilage in the specimens from degrading (22). A spatial resolution with an isotropic voxel size of 8 μm (matrix 2048 × 2048, 1000 projections/180°, FOV 16.4 mm) was utilized. Specimens were scanned along the length of each core, encompassing the vertebral endplate surface and 3 mm of bone underneath it. Image cross sections were restored to a 3D structure using the manufacturers' cone beam reconstruction algorithm (23) and then each 3D structure was transformed into 1000–1100 serial 8 μm thick sliced images in a sagittal orientation. Next, a light Gaussian filter (to remove high frequency noise) followed by a fixed threshold (to binarize the images into a bone and pore phase) was applied to each sagittal slice. The irregular vertebral endplate surface was then identified using a custom algorithm developed using MATLAB software. The semiautomatic technique is fully described elsewhere (24).

Four bone microstructural indices, pore fraction (PF [%]), trabecular thickness (Tb.Th [mm]), pore diameter (Po.Dm [mm]) and pore number (Po.N [1/mm]) were obtained. PF was calculated by voxel counting, while Tb.Th, Po.Dm and Po.N were calculated using a 3D distance transformation method (25). The distance transformation method calculates the distance of every bone/voxel (object) to the nearest bone/air (background) surface. The distances were visualized as the radius of a sphere with a center in the voxel that fits inside each bone structure. Then, the redundant spheres were removed and the largest spheres confined the smaller spheres. This resulted in the mid axes of the maximal spheres filling the structure completely (25). To calculate pore fraction (porosity), data from the binarized images mentioned above was used to calculate the fraction of pore volume per tissue volume or (1-BV/TV, where BV is bone volume and TV is total volume). Next, to calculate Tb.Th, each trabeculae attained the value of the radius of the maximal sphere contained in the trabecular bone. Then, the mean value of the diameter (twice the radius) was assigned as the Tb.Th. The calculation of Po.Dm followed the same procedure except each voxel in the background (saline) was fitted with a maximal sphere instead of the bone. Then, the distance between the spheres' mid axes was calculated and the inverse was taken to provide the number of pores per mm, Po.N.

In order to assess spatial changes in endplate morphology, four regions of interest (ROIs) were defined (Figure 1B). Initially, the cylinder lateral boundaries were defined in the μCT dataset by an interpolation across the slices of two circles placed at the superior and inferior ends of the specimen. This bounded the sides of each of the four ROIs. The endplate surface contour was computed on a slice-by-slice basis using Bezier splines (26) to conform a 3D mesh. A local valley detection algorithm was implemented to bridge surface pores along the initial spline (27). These splines composed the top and bottom ROI surfaces that were parallel to the subchondral bone surface within each sagittal μCT image forming the four ROIs (Figure 2). The top endplate surface spline was propagated down into the sample to various depths. The endplate surface ROI was identified as a 16 μm (two pixels) thick region underlying the surface contour. A second 16 μm thick ROI (most-dense) was located at the site of maximum bone density. The third ROI, defined as the vertebral endplate thickness (VEP Th), was the region from the surface contour to the point of maximum bone density. The fourth ROI consisted of the region from the subchondral surface to a depth of 2 mm. This thickness was also used in previous studies (28).

The hydraulic permeability of the cores was measured using a custom permeameter as described previously(29). Briefly, this included measuring the change in flow rate of saline, physiologically pressurized so that the driving hydraulic pressure was against the cartilage endplate thus the fluid passed in the "flow-out" disc to bone direction, perpendicular to the endplate surface and along the length of the core. These experiments determined the

permeability of the entire specimen and of the endplate cartilage and subchondral bone separately.

The nuclear tissue was separated in three parts to determine the difference in cell density and GAG content within the disc. Each part of the tissue was obtained by digesting the nuclear tissue and separating it into the supernatant and pellet. The GAG content was quantified from the supernatant using the DMMB assay and the cell density was calculated from the DNA content obtained from the pellet using the PicoGreen assay.

Statistical analyses were performed using a commercial statistical software package (JMP v5.0, SAS Institute, Inc., Cary, NC). Analysis of variance (ANOVA) procedures were used to calculate group means and to test for differences in the microstructural indices between bone regions. Donor age was included as a covariate. When indicated, a post-hoc Tukey test was performed. Regression analyses were also performed to estimate the effects of the structural bone indices at each of the four ROIs on degeneration grade, cell density, GAG content, total permeability, bone permeability and cartilage permeability.

Results

Six cores were excluded due to severe, degeneration-related inhomogeneities at the surface that could not be analyzed in a semiautomatic fashion. The number of cores was divided in the following groups: [n=96 from 14 subjects L1–L5, degeneration grade 1 (n=4), grade 2 (n=32), grade 3 (n=44), grade 4(n=10), grade 5(n=6). Overall, porosity varied significantly between ROIs. The 2 mm ROI had the highest porosity (69% ± 9) followed by the surface ROI (54% ± 8), the VEP Th (44% ±14) and the most-dense ROI (43% ± 16) (Table 1). Po.N was highest at the surface and lowest at the 2 mm region.

Degeneration effects

The 2 mm region was more porous than the other three regions for healthy, grade 1 discs ($p<0.05$). With increasing degeneration the porosity at each of the ROIs increased significantly, except for 2 mm region (Figure 3). For the most-dense and VEP thickness ROIs, trabecular thickness had statistically significant decrease with degeneration ($p<0.05$; Figure 4). As expected, the most-dense ROI contained the thickest trabeculae for grade 1 samples, where the trabecular thickness was approximately twice that at the endplate surface. This large difference decreased as the adjacent discs became more degenerated (grade 1 to grade 5). All the regions except for the 2 mm region had statistically significant variations with degeneration grade. For grade 1 discs, the smallest pore diameter was located at the vertebral surface region ($p<0.05$), but for grade 5 discs, differences in pore diameter as a function of depth were not statistically apparent ($p>0.2$). Overall, pore diameter at the surface region and the most-dense region were dependent on degeneration grade, where the pore diameter increased as the adjacent disc became more degenerated. This dependence was statistically significant. The first four degeneration grades showed statistically significant differences between the four regions. These differences in pore number were not observed in the four regions at grade 5.

Structural bone indices variation with age, GAGs and cell density

Since no statistically significant difference was observed between the three parts of the nuclear tissue in a previous study(29), the average cell density and GAG content was used. Nucleus GAG content decreased as age increased, while porosity and pore diameter increased in all four regions (Table 2). In addition, as age increased, trabecular thickness and pore number decreased. Nucleus cell density increased with age as the endplate became

more porous with thinner trabeculae. Overall, the structural bone indices followed similar age-related trends in all 4 ROIs.

Permeability

The total, cartilage, and bone permeability tended to increase with an increase in bone porosity and with a decrease in trabecular thickness in the four regions (Table 2). These consistent trends in the four regions were not observed between the three permeabilities and pore diameter and pore number. Statistically significant trends with total, bone and cartilage permeability in at least one region for all indices were observed.

Additional Observations

Twenty-three percent (22/96) cores demonstrated ‘double endplates’ that was most common adjacent to degenerated discs grade 2 or 3 (Figure 5). The majority of the double layer-vertebral endplate specimens were observed from three donors in both superior and inferior vertebral bodies of the L1–L5 levels including 13 IVDs, 16 vertebral cores out of 27 possible vertebral cores showed this feature (Figure 5). These three donors were males in the 49–84 years age range.

Discussion

Our data demonstrate significant depth-dependent changes in endplate bone morphology, with the peak density occurring at approximately 0.29 ± 0.20 mm below the endplate surface. However, this heterogeneity decreased with increasing disc degeneration. Morphological features correlated with three adjacent disc degeneration indicators (Pfirrmann grade, cell density and GAG content) as well as with permeability. In general, the endplate became thinner and more porous with age and degeneration.

The VEP changes from a heterogeneous structure to a homogeneous structure as the adjacent disc degenerates. This indicates that while bone loss occurs throughout the VEP with an increased in age, density is lost predominantly in the most-dense region. Adjacent to grade 1 discs, porosity, trabecular thickness and pore diameter were lowest in the surface region. This difference disappeared for endplates adjacent to grade 5 discs. Therefore, changes occurring to the denser regions are more pronounced, manifested as a higher rate, than the surface and the 2 mm regions (Figure 6). The loss of endplate heterogeneity is consistent with prior reports that vertebral bone structure is more heterogeneous in young human lumbar vertebrae than in older ones (30). Overall, bone loss lead to an increased surface porosity suggesting that sclerosis does not accelerate degeneration as others had hypothesized (12, 13). While it has been reported that sclerosis has a higher likelihood to appear in the periphery of the vertebra (31), computational studies indicate that the periphery does not appear to interfere with the main nutrient diffusion path for nucleus pulposus cells(20).

Nucleus cell density correlated with the endplate morphological indices, indicating an increase in cell density as the VEP became more porous. These results did not support the notion that endplates become more sclerotic with age, compromised disc cell nutrition, and thereby promote degenerative change. We have previously demonstrated that disc cell density is more strongly correlated with disc height, and tends to increase with the later stages of degeneration when discs collapse due to GAG loss(29). Yet, though disc cell density tends to increase, these cells become less synthetically active which may be due to senescence or other factors such as changes in the osmotic environment or the presence of inflammatory factors (32).

Though we did not observe a correlation between endplate sclerosis and disc degeneration, a lack of nutrient availability may still be an important degenerative factor. Previous studies demonstrate that vertebral perfusion decreases with age. For example, using contrast-enhanced MRI, Montazel and coworkers show that vertebral blood flow decreases by almost 75% between ages 30 and 60 (6, 7, 33, 34). Using similar techniques, Liu and colleagues demonstrate that perfusion is decreased by 14% in vertebra adjacent to degenerated discs (35). Vertebral blood supply is dependent on hematopoietic marrow (36) that gradually converts to fat at a rate of approximately 6% per decade. During this transformation, thin-walled vascular sinusoids are replaced by capillaries (37) with thicker walls that decrease the effective perfusion (38). Additionally, the growth of fat cells in the rigid intraosseous compartment can increase pressure and compress vessels, further decreasing blood flow (39).

In accordance with previous studies, we observed a decrease in vertebral endplate thickness with degeneration (11, 40). A double endplate structure, noted by others, was also detected in a subset of our samples (41). This feature was observed only on vertebral cores adjacent to Pfirrmann grade 2 and 3 discs, which might suggest that this is a transient feature that is lost as the endplate surface subsides toward the periphery with degeneration. Interestingly, the majority of the double layer features were observed in male donors, supporting the suggestion of different bone distributions occurring in males and females(42).

Previous studies characterizing vertebral endplate bone focus on interactions between disc degeneration and vertebral stiffness (16, 31), or on endplate compatibility with devices and techniques for spinal fusion (15). Yet, these prior data are consistent with our observations. For example, Grant and coworkers report that endplate indentation strength is decreased by between 30% and 60% in more degenerated discs, which compares well to our approximate 50% increase in endplate surface porosity. Beyond traditional mechanical parameters such as stiffness and strength, the current study is one of few that compares endplate morphological changes with adjacent disc degeneration (40). We used a high spatial resolution μCT to study the morphology at the level of individual trabeculae within the vertebra. The semiautomatic selection method chose predetermined regions in a systematic fashion. The focus on the microscale provides more details about the changes occurring in the VEP with degeneration. A study limitation is the focus on the central endplate and consequently, the results may not be applicable to the vertebral rim. Another limitation is the nature of cadaveric studies that preclude conclusions regarding cause-and-effect. As a result, we can only speculate about the potential mechanisms driving the bone morphology changes and adjacent disc degeneration.

Our results suggest that measures of endplate morphology may add value to current regimens that rate degenerative status. Currently, pain level and disc degeneration grades are used for assessment of appropriate interventions which may require surgery (43). Additional degeneration information based on the VEP morphology could potentially increase the accuracy of the degeneration assessment. While μCT is inappropriate for human use because of the high radiation dose, the results may be translated to clinical devices such as DXA and MRIs using registration techniques (44).

Overall, this study provides new information regarding endplate morphology, its changes with age, and its potential role in disc degeneration. The increase in bone porosity in the vertebral endplate with Pfirrmann grade, GAG content, and age suggests that nutrient diffusion is not interrupted by endplate sclerosis. Rather it suggests that the potential barriers to disc nutrition could be driven by changes in either cell function (45, 46) or vertebral capillary density (47). Future studies may explore whether a reduction in capillary density at

the VEP reduces the vertebral blood supply of nutrients available to the disc leading to disc degeneration.

Acknowledgments

NIH Grant: RO1AR052811

References

1. Andersson GB. Epidemiology of low back pain. Acta Orthop Scand Suppl. 1998; 281:28–31. [PubMed: 9771538]
2. Freemont AJ, Watkins A, Le Maitre C, et al. Current understanding of cellular and molecular events in intervertebral disc degeneration: implications for therapy. J Pathol. 2002; 196(4):374–9. [PubMed: 11920731]
3. Buckwalter JA. Spine Update: Aging and degeneration of the Human Intervertebral Disc. Spine. 1995; 20(11):1307–14. [PubMed: 7660243]
4. Nerlich AG, Schleicher ED, Boos N. 1997 Volvo Award winner in basic science studies. Immunohistologic markers for age-related changes of human lumbar intervertebral discs. Spine. 1997; 22(24):2781–95. [PubMed: 9431614]
5. Videman T, Battie MC. The influence of occupation on lumbar degeneration. Spine (Phila Pa 1976). 1999; 24(11):1164–8. [PubMed: 10361670]
6. Boos N, Weissbach S, Rohrbach H, et al. Classification of age-related changes in lumbar intervertebral discs: 2002 Volvo Award in basic science. Spine. 2002; 27(23):2631–44. [PubMed: 12461389]
7. Nachemson A, Lewin T, Maroudas A, et al. In vitro diffusion of dye through the end-plates and the annulus fibrosus of human lumbar inter-vertebral discs. Acta Orthop Scand. 1970; 41(6):589–607. [PubMed: 5516549]
8. Urban JP, Holm S, Maroudas A. Diffusion of small solutes into the intervertebral disc: as in vivo study. Biorheology. 1978; 15(3–4):203–21. [PubMed: 737323]
9. Horner HA, Urban JP. 2001 Volvo Award Winner in Basic Science Studies: Effect of nutrient supply on the viability of cells from the nucleus pulposus of the intervertebral disc. Spine. 2001; 26(23):2543–9. [PubMed: 11725234]
10. Roberts S, Caterson B, Evans H, et al. Proteoglycan components of the intervertebral disc and cartilage endplate: an immunolocalization study of animal and human tissues. Histochem J. 1994; 26(5):402–11. [PubMed: 7519184]
11. Bernick S, Cailliet R. Vertebral end-plate changes with aging of human vertebrae. Spine. 1982; 7(2):97–102. [PubMed: 7089697]
12. Kokkonen SM, Kurunlahti M, Tervonen O, et al. Endplate degeneration observed on magnetic resonance imaging of the lumbar spine: correlation with pain provocation and disc changes observed on computed tomography diskography. Spine. 2002; 27(20):2274–8. [PubMed: 12394906]
13. Roberts S, Evans H, Trivedi J, et al. Histology and pathology of the human intervertebral disc. J Bone Joint Surg Am. 2006; 88 (Suppl 2):10–4. [PubMed: 16595436]
14. Aoki J, Yamamoto I, Kitamura N, et al. End plate of the discovertebral joint: degenerative change in the elderly adult. Radiology. 1987; 164(2):411–4. [PubMed: 3602378]
15. Grant JP, Oxland TR, Dvorak MF, et al. The effects of bone density and disc degeneration on the structural property distributions in the lower lumbar vertebral endplates. J Orthop Res. 2002; 20(5):1115–20. [PubMed: 12382980]
16. Keller TS, Ziv I, Moeljanto E, et al. Interdependence of lumbar disc and subdiscal bone properties: a report of the normal and degenerated spine. J Spinal Disord. 1993; 6(2):106–13. [PubMed: 8504221]
17. Banse X, Devogelaer JP, Munting E, et al. Inhomogeneity of human vertebral cancellous bone: systematic density and structure patterns inside the vertebral body. Bone. 2001; 28(5):563–71. [PubMed: 11344057]

18. Simpson AK, Biswas D, Emerson JW, et al. Quantifying the effects of age, gender, degeneration, and adjacent level degeneration on cervical spine range of motion using multivariate analyses. Spine. 2008; 33(2):183–6. [PubMed: 18197104]
19. Pfirrmann CW, Metzdorf A, Zanetti M, et al. Magnetic resonance classification of lumbar intervertebral disc degeneration. Spine. 2001; 26(17):1873–8. [PubMed: 11568697]
20. Soukane DM, Shirazi-Adl A, Urban JP. Computation of coupled diffusion of oxygen, glucose and lactic acid in an intervertebral disc. J Biomech. 2007; 40(12):2645–54. [PubMed: 17336990]
21. Arramon, YP.; Nauman, EA. The Intrinsic Permeability of Cancellous Bone. In: Cowin, S., editor. Bone Mechanics Handbook. 2. CRC Publishing; 2001.
22. Setton LA, Zhu W, Weidenbaum M, et al. Compressive properties of the cartilaginous end-plate of the baboon lumbar spine. J Orthop Res. 1993; 11(2):228–39. [PubMed: 8483035]
23. Nazarian A, Snyder BD, Zurakowski D, et al. Quantitative micro-computed tomography: a non-invasive method to assess equivalent bone mineral density. Bone. 2008; 43(2):302–11. [PubMed: 18539557]
24. Rodriguez, AG. Human endplate permeability and microstructure and their relationship to disc degeneration: University of California. San Francisco with the University of California; Berkeley: 2010.
25. Hildebrand T, Ruegsegger P. A new method for the model-independent assessment of thickness in three-dimensional images. Journal of Microscopy. 1997; 185:67–75.
26. Carballido-Gamio J, Link TM, Majumdar S. New techniques for cartilage magnetic resonance imaging relaxation time analysis: texture analysis of flattened cartilage and localized intra- and inter-subject comparisons. Magn Reson Med. 2008; 59(6):1472–7. [PubMed: 18506807]
27. Lu W, Nystrom MM, Parikh PJ, et al. A semi-automatic method for peak and valley detection in free-breathing respiratory waveforms. Med Phys. 2006; 33(10):3634–6. [PubMed: 17089828]
28. Sylvestre PL, Villemure I, Aubin CE. Finite element modeling of the growth plate in a detailed spine model. Med Biol Eng Comput. 2007; 45(10):977–88. [PubMed: 17687580]
29. Rodriguez AG, Slichter CK, Acosta FL, et al. Human disc nucleus properties and vertebral endplate permeability. Spine (Phila Pa 1976). 2011; 36(7):512–20. [PubMed: 21240044]
30. Thomsen JS, Ebbesen EN, Mosekilde L. Zone-dependent changes in human vertebral trabecular bone: clinical implications. Bone. 2002; 30(5):664–9. [PubMed: 11996902]
31. Harada A, Okuizumi H, Miyagi N, et al. Correlation between bone mineral density and intervertebral disc degeneration. Spine (Phila Pa 1976). 1998; 23(8):857–61. discussion 62. [PubMed: 9580951]
32. Le Maitre CL, Pockert A, Buttle DJ, et al. Matrix synthesis and degradation in human intervertebral disc degeneration. Biochem Soc Trans. 2007; 35(Pt 4):652–5. [PubMed: 17635113]
33. Montazel JL, Divine M, Lepage E, et al. Normal spinal bone marrow in adults: dynamic gadolinium-enhanced MR imaging. Radiology. 2003; 229(3):703–9. [PubMed: 14593190]
34. Urban JP, Winlove CP. Pathophysiology of the intervertebral disc and the challenges for MRI. J Magn Reson Imaging. 2007; 25(2):419–32. [PubMed: 17260404]
35. Liu YJ, Huang GS, Juan CJ, et al. Intervertebral disk degeneration related to reduced vertebral marrow perfusion at dynamic contrast-enhanced MRI. AJR Am J Roentgenol. 2009; 192(4):974–9. [PubMed: 19304703]
36. Whitby, LEH.; Britton, CJC. Disorders of the blood. 10. New York: Grune and Stratton; 1969.
37. Burkhardt R, Kettner G, Bohm W, et al. Changes in trabecular bone, hematopoiesis and bone marrow vessels in aplastic anemia, primary osteoporosis, and old age: a comparative histomorphometric study. Bone. 1987; 8(3):157–64. [PubMed: 3606907]
38. Kricun ME. Red-yellow marrow conversion: its effect on the location of some solitary bone lesions. Skeletal Radiol. 1985; 14(1):10–9. [PubMed: 3895447]
39. Drescher W, Li H, Qvesel D, et al. Vertebral blood flow and bone mineral density during long-term corticosteroid treatment: An experimental study in immature pigs. Spine (Phila Pa 1976). 2000; 25(23):3021–5. [PubMed: 11145813]

40. Roberts S, McCall IW, Menage J, et al. Does the thickness of the vertebral subchondral bone reflect the composition of the intervertebral disc? Eur Spine J. 1997; 6(6):385–9. [PubMed: 9455665]

41. Edwards WT, Zheng Y, Ferrara LA, et al. Structural features and thickness of the vertebral cortex in the thoracolumbar spine. Spine. 2001; 26(2):218–25. [PubMed: 11154545]

42. Limthongkul W, Karaikovic EE, Savage JW, et al. Volumetric analysis of thoracic and lumbar vertebral bodies. Spine J. 2010; 10(2):153–8. [PubMed: 20142072]

43. Don AS, Carragee E. A brief overview of evidence-informed management of chronic low back pain with surgery. Spine J. 2008; 8(1):258–65. [PubMed: 18164474]

44. MacNeil JA, Boyd SK. Accuracy of high-resolution peripheral quantitative computed tomography for measurement of bone quality. Med Eng Phys. 2007; 29(10):1096–105. [PubMed: 17229586]

45. Holm S, Nachemson A. Nutrition of the intervertebral disc: acute effects of cigarette smoking. An experimental animal study. Ups J Med Sci. 1988; 93(1):91–9. [PubMed: 3376356]

46. Oda H, Matsuzaki H, Tokuhashi Y, et al. Degeneration of intervertebral discs due to smoking: experimental assessment in a rat-smoking model. J Orthop Sci. 2004; 9(2):135–41. [PubMed: 15045541]

47. Rajasekaran S, Babu JN, Arun R, et al. ISSLS prize winner: A study of diffusion in human lumbar discs: a serial magnetic resonance imaging study documenting the influence of the endplate on diffusion in normal and degenerate discs. Spine (Phila Pa 1976). 2004; 29(23):2654–67. [PubMed: 15564914]

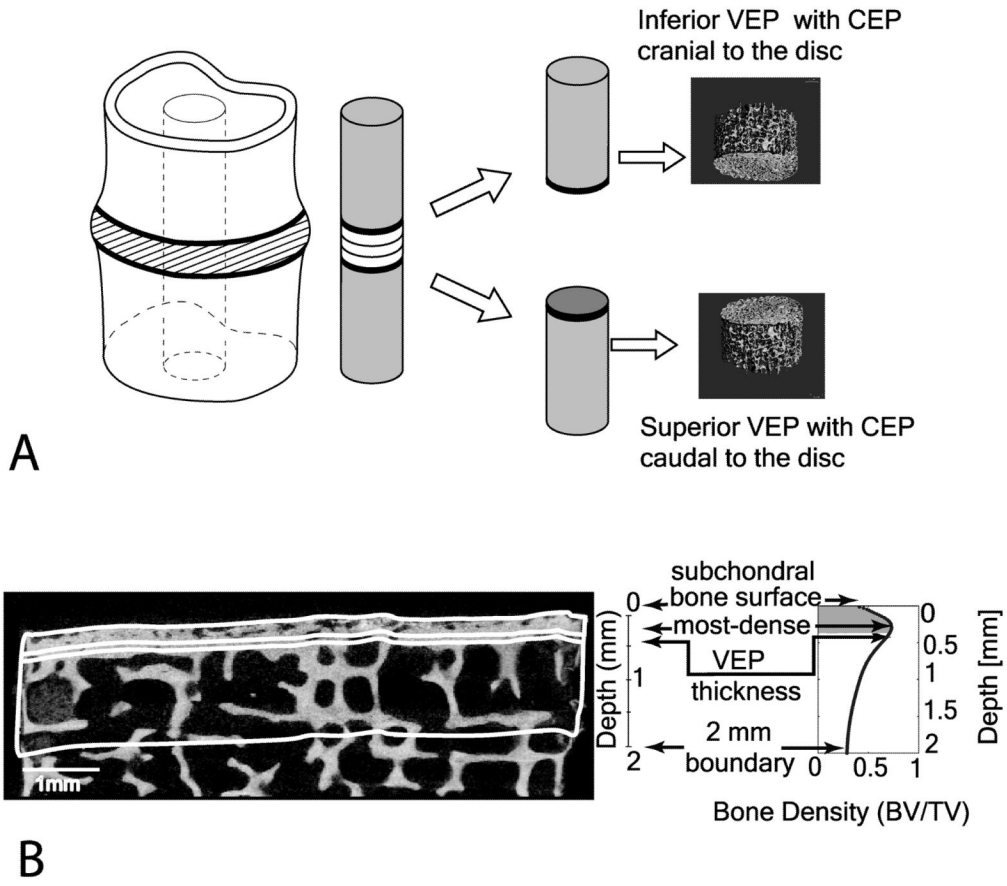

Figure 1.

(A) (From left to right). The diagram shows the cylindrical core obtained from the vertebral motion segment. It is followed by a 3D MicroCT image of the two individual vertebral cores highlighting the location of the 2 mm regions. From the surface, a 2 mm thick region was selected. (B) A sagittal binarized image of a subchondral bone section with a 2 mm ROI was selected (bottom left). A plot of the bone volume fraction (BV/TV) variation through the 2 mm depth is shown on the right. The location of the four ROIs analyzed was matched visually with the sagittal image on the left (bottom right).

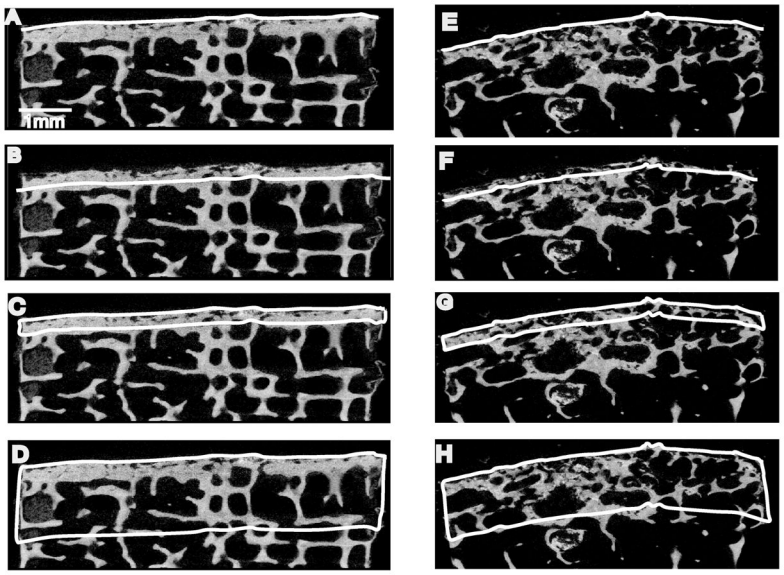

Figure 2.
MicroCT binarized sagittal sections from two specimens. The left column shows ROIs for a vertebral core next to a healthy disc and the right shows a vertebral core next to degenerated disc. A & E highlight the ‘surface’ region; B & F highlight the ‘most-dense’ region. C & G highlight the ‘VEP thickness’ region and D & H highlight the ‘2 mm’ region.

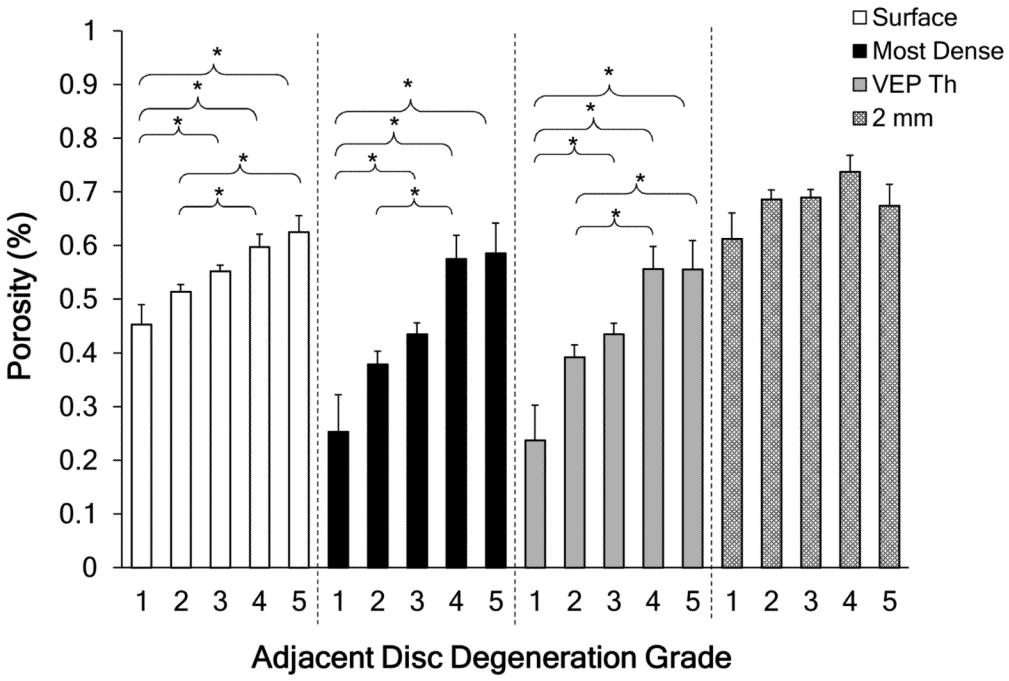

Figure 3.

Porosity variations with degeneration over the four regions. * = statistically significant difference ($p<0.05$). Error bars represent one standard deviation. Degeneration grade 1 (n=4), grade 2 (n=32), grade 3 (n=44), grade 4(n=10), grade 5 (n=6).

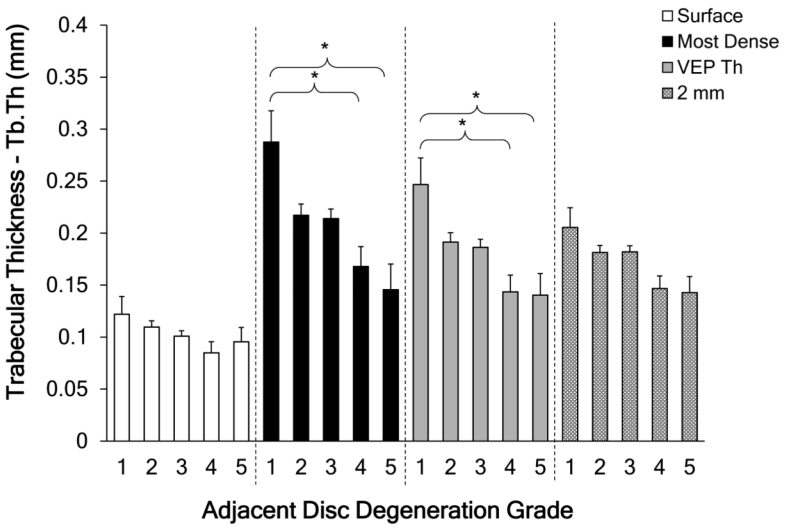

Figure 4.

Trabecular thickness variations with degeneration over the 4 regions. * = statistically significant difference ($p<0.05$). Error bars represent one standard deviation. Degeneration grade 1 (n=4), grade 2 (n=32), grade 3 (n=44), grade 4(n=10), grade 5 (n=6).

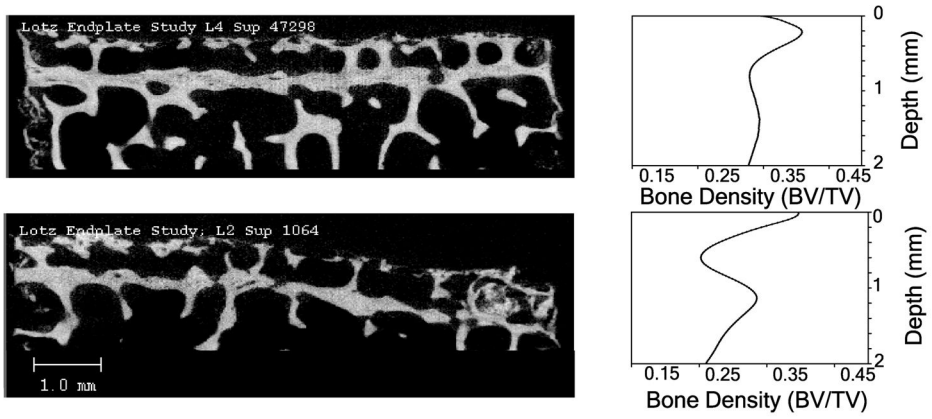

Figure 5.

Sagittal slices of two samples that showed a double layer vertebral endplate (left). The matching bone density distribution per depth is presented (right). On the top left, level L4 superior vertebral endplate is shown and on the bottom left, level L2 superior vertebral endplate is shown. Each sample's distribution of bone density vs. depth plot is shown on the right. The double layer endplate can be seen in the plots on the right as showing two separate peaks.

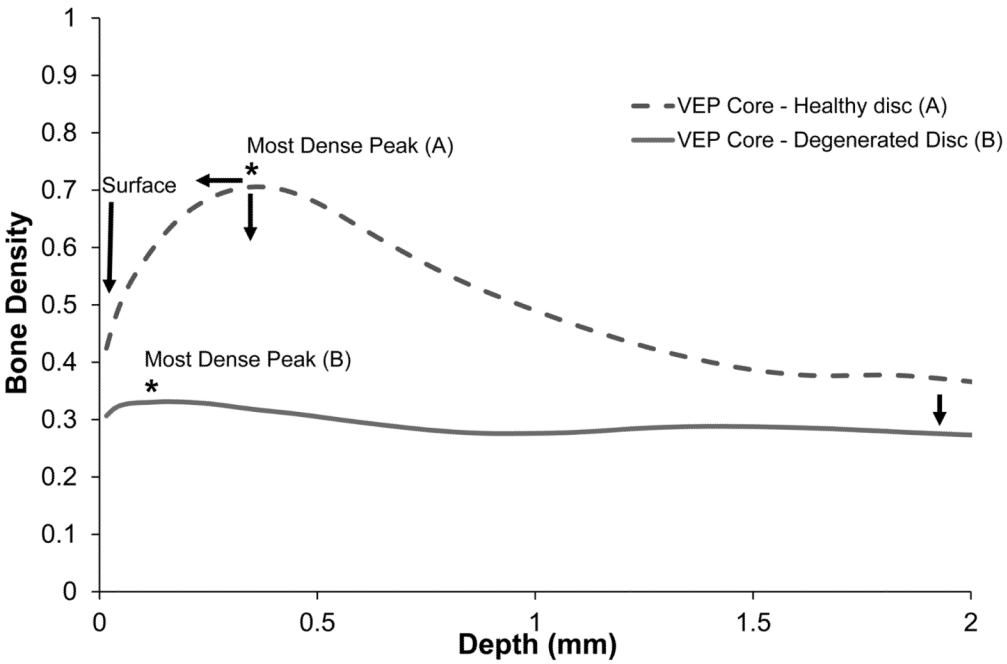

Figure 6.

Degeneration changes from two representative vertebral cores: (A) adjacent to a healthy disc and (B) adjacent to a degenerative disc, are illustrated showing a bone density variation in 2 mm depth. As the disc adjacent to a vertebral endplate became more degenerated (sample B). The most-dense peak moved closer to the surface and the bone density decreased with degeneration. The quantity of trabeculae below the transitional zone (most dense peak) also decreased as the disc became more degenerated.

Table 1

The average (Ave) and standard deviations (SD) for each structural index in all four regions

Structural Bone Indices	Regions	Average	±SD	Grade 1 (n=4)	Grade 2 (n=32)	Grade 3 (n=44)	Grade 4 (n=10)	Grade 5 (n=6)
				Ave±SD	Ave±SD	Ave±SD	Ave±SD	Ave±SD
PF	Surface	54%	8	0.43±.04	0.51±.01	0.55±.01	0.60±.02	0.63±.03
	Most Dense	43%	16	0.26±.07	0.38±.02	0.43±.02	0.58±.04	0.59±.06
	VEP Th	44%	14	0.24±.07	0.39±.02	0.43±.02	0.56±.04	0.56±.05
	2 mm	69%	9	0.62±.05	0.69±.02	0.69±.01	0.74±.03	0.67±.04
Tb.Th	Surface	0.10 mm	0.02	0.12±.02	0.11±.01	0.10±.01	0.08±.01	0.10±.01
	Most Dense	0.21 mm	0.06	0.29±.03	0.22±.01	0.21±.01	0.17±.02	0.15±.02
	VEP Th	0.18 mm	0.05	0.25±.03	0.19±.01	0.19±.01	0.14±.02	0.14±.02
	2 mm	0.17 mm	0.04	0.21±.02	0.18±.01	0.18±.01	0.15±.01	0.14±.02
Po.Dm	Surface	0.19 mm	0.09	0.14±.03	0.15±.01	0.18±.01	0.29±.02	0.32±.03
	Most Dense	0.33 mm	0.08	0.25±.04	0.31±.02	0.35±.01	0.39±.03	0.33±.03
	VEP Th	0.24 mm	0.08	0.17±.04	0.20±.01	0.24±.01	0.33±.02	0.32±.03
	2 mm	0.53 mm	0.12	0.42±.06	0.53±.02	0.53±.02	0.57±.04	0.45±.05
Po.N	Surface	6.24/mm	1.12	6.00±.50	6.75±.18	6.27±.15	5.75±.32	4.57±.41
	Most Dense	4.36/mm	1.46	6.98±.80	4.75±.28	4.10±.24	4.03±.50	4.52±.65
	VEP Th	4.27/mm	0.69	3.83±.35	4.32±.12	4.23±.12	4.53±.22	4.24±.28
	2 mm	2.88/mm	0.52	2.96±.25	2.81±.09	2.86±.07	2.98±.16	3.40±.20

PF = pore fraction (%); Tb.Th = trabecular thickness (mm), Po.Dm = pore diameter (mm); Po.N = pore number (1/mm); VEP Th = vertebral endplate thickness.

Table 2

Correlations of structural bone indices with GAG, cell density, total permeability, bone permeability and cartilage permeability for each of the four regions and controlled for age.

Structural Bone Index	Regions	Trend	GAG	Trend	Cell Density	Trend	Total Permeability	Trend	Bone Permeability	Trend	Cartilage Permeability
PF	Surface	↓	0.21*	↓	0.16 *	↑	0.19	↑	0.32 *	↑	0.17 *
	Most Dense	↓	0.26*	↓	0.25 *	↑	0.28 *	↑	0.36 *	↑	0.26 *
	VEP Th	↓	0.35 *	↓	0.33 *	↑	0.29 *	↑	0.46 *	↑	0.28 *
	2 mm	↓	0.47 *	↓	0.41 *	↑	0.33 *	↑	0.34 *	↑	0.28 *
Tb.Th	Surface	↑	0.13 *	↑	0.13 *	↓	0.28 *	↓	0.25 *	↓	0.33 *
	Most Dense	↑	0.26 *	↑	0.25 *	↓	0.27 *	↓	0.33 *	↓	0.26 *
	VEP Th	↑	0.28 *	↑	0.26 *	↓	0.29 *	↓	0.31 *	↓	0.28 *
	2 mm	↑	0.23 *	↑	0.23 *	↓	0.30 *	↓	0.25 *	↓	0.28 *
Po.Dm	Surface	↓	0.16 *	↑	0.22 *	→	0.10	↑	0.21 *	→	0.08
	Most Dense	↓	0.22 *	↑	0.17 *	→	0.15	↑	0.14	→	0.12
	VEP Th	↓	0.2 *	↑	0.24 *	→	0.18	↑	0.32 *	→	0.16
	2 mm	↓	0.42 *	↑	0.35 *	↑	0.24 *	↑	0.21 *	→	0.23 *
Po.N	Surface	→	0.14 *	↓	0.15 *	→	0.04	→	0.08	→	0.06
	Most Dense	↑	0.2 *	↑	0.2 *	→	0.19	→	0.22 *	→	0.19 *
	VEP Th	↑	0.1	↓	0.15 *	↑	0.23 *	↑	0.13	→	0.21 *
	2 mm	↑	0.19 *	→	0.06	→	0.08	→	0.02	→	0.04

* = statistically significant difference ($p<0.05$). (↑) increasing trend, (↓) decreasing trend and (→) no relationship. The arrow indicate the trend that age, GAGs, cell density total, bone or cartilage permeability (dependent variables) follow with bone index (independent variable). PF = pore fraction (%); Tb.Th = trabecular thickness (mm), Po.Dm = pore diameter (mm); Po.N = pore number (1/mm); VEP Th = vertebral endplate thickness.